

# Robotic Nonprehensile Object Transportation with a Hanging Tray

Adam Heins  
University of Toronto  
Toronto, Canada

adam.heins@robotics.utias.utoronto.ca

Angela P. Schoellig  
Technical University of Munich  
Munich, Germany  
angela.schoellig@tum.de

**Abstract**—We consider the nonprehensile object transportation task known as the *waiter’s problem*, in which a robot must move an object balanced on a tray from one location to another. In contrast to prior works on the robotic waiter’s problem, which make the robot tilt a tray *rigidly held* by its end effector (EE), we use a tray *suspended* from the EE by ropes, such that it behaves like a three-dimensional pendulum. Some prior works have actuated the robot so that the EE *simulates* the behavior of a pendulum, because pendular motion reduces the shear forces acting on the transported objects, minimizing the sliding of rigid objects and sloshing in containers of liquid. In contrast, our use of a *real* hanging tray allows us to obtain the benefits of pendular motion while only actuating a 3 degree-of-freedom (DOF) mobile base, rather than requiring a full 6-DOF manipulator arm. Our experiments in simulation and on real hardware show that the hanging tray substantially reduces both sliding and sloshing compared to a static, rigidly-grasped tray. Furthermore, we integrate the hanging tray into an interactive robot waiter demonstration, which uses computer vision to identify people with a raised hand and visual servoing to steer toward them and allow them to access the tray.

## I. INTRODUCTION

The *waiter’s problem* [1] is a nonprehensile manipulation task that requires a robot to transport objects balanced on a tray, like a restaurant waiter. Nonprehensile manipulation [2] occurs when the manipulated objects are not rigidly grasped, such that they retain some independent degrees of freedom (DOFs). In the waiter’s problem, the objects are only attached to the tray by frictional contact, and thus it is possible for them to slide or tip unless the motion of the robot is designed to avoid it. Other examples of nonprehensile manipulation include pushing, rolling, and throwing [3], [4]. Solving the waiter’s problem is appealing because the use of a tray avoids the need to grasp and ungrasp each object, allows many objects to be transported at once, and can handle delicate objects which may be difficult to grasp at all [5]. It may be useful for transporting objects in industries including food service, warehouse fulfillment, and manufacturing.

In contrast to previous approaches to the robotic waiter’s problem, which tilt a tray *rigidly attached* to the robot’s end effector (EE), we borrow an idea from human waiters (e.g., the Moroccan tea service [6]) and *suspend* the tray from ropes, allowing it to swing freely like a three-dimensional (3D) pendulum. The swinging naturally reduces the shear forces acting on the transported objects, therefore requiring less

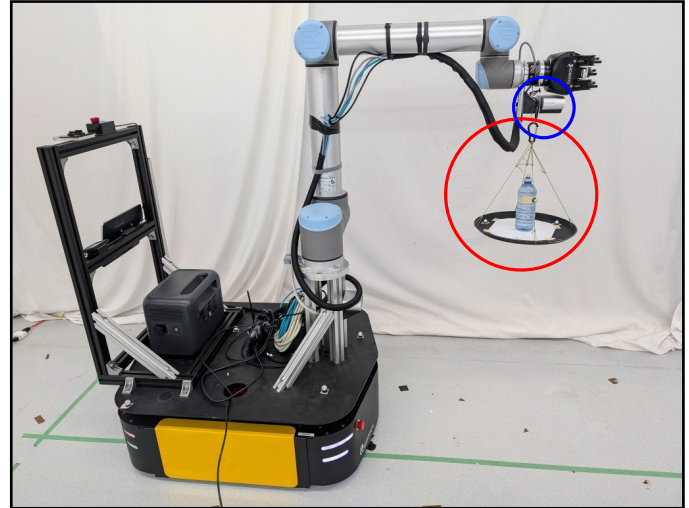


Figure 1: We present the first work on robotic nonprehensile object transportation that uses a real hanging tray (circled red) to support the transported objects. A key benefit is that an actuated manipulator arm is not necessary: in all of our experiments, we keep the arm stationary and only actuate the mobile base, allowing the swinging of the tray to naturally prevent the objects from sliding. An RGB-D camera (circled blue) allows the robot to detect human gestures and steer toward people to serve them. A video of the experiments can be found at <http://tiny.cc/visual-servor>.

friction to prevent the objects from sliding. A key benefit of this approach is that the robot can move quickly without needing to rotate the EE to prevent sliding. Indeed, in our experiments on the robot shown in Fig. 1, we only control the mobile base and do not require any actuation of the manipulator arm. Once the robot reaches its destination, the swinging of the tray is rapidly damped out using a linear quadratic regulator (LQR).

In addition, we integrate the hanging tray into an interactive robot waiter demonstration that uses an RGB-D camera to detect and serve people like a waiter. In particular, we use a convolutional neural network (CNN) to detect people raising their hands, indicating that they would like to be served. The robot then uses visual servoing to steer toward them. When the robot reaches the person, it damps out the swinging of the tray, waits a fixed amount of time for the person to take the desired item from the tray, and then returns to its original position until another person gestures to it. This is the first time that gesture-based visual servoing has been used explicitly for the waiter’s problem.

In summary, the main contributions of this work are:

- the first use of a real hanging tray for robotic nonprehensile object transportation, including modelling, analysis, and hardware experiments;
- a novel interactive robot waiter demonstration that combines the hanging tray with gesture recognition and visual servoing to interactively serve people, demonstrated on a real mobile manipulator;
- an open-source implementation of our code, available at [https://github.com/learnsyslab/visual\\_servor](https://github.com/learnsyslab/visual_servor).

## II. RELATED WORK

The waiter’s problem has been approached using a variety of methods including offline planning [5], [7]–[9], online planning (i.e., model predictive control) [10], [11], and reactive control [12]–[15]. Broadly, all of these methods try to tilt the tray so that the shear forces acting on the transported object are small, and therefore friction can balance them out and prevent the object from sliding. However, this at least requires the actuated DOFs to tilt the tray, and may also require an object model that includes geometry and inertial parameters.

One interesting approach is to simulate the motion of a pendulum with the robot’s EE, which naturally minimizes shear forces acting on the transported object without explicitly modelling it. This was first done in [6] with a parallel manipulator mounted on a mobile robot, but only in two dimensions. This idea was extended to the three-dimensional case [12], [13] to minimize slosh when transporting liquids with a fixed-base manipulator arm. Inspired by these approaches, we use a real, physical pendulum rather than simulating one. That is, we *suspend* the tray from the EE so that it can swing freely, which means we do not need an actuated arm to tilt the tray nor do we need models of the transported objects. Our proposed approach is similar to the commercial SpillNot product [16], which is a suspended tray designed for carrying cups of liquid without spilling them. However, we are the first to use a suspended tray for nonprehensile object transportation on a robot, which presents the additional challenge of damping out the unwanted swinging of the tray once the robot reaches its destination. To do so, we design an LQR-based controller similar to [17], except that we also introduce an integral term to eliminate the steady-state position error that occurs when the pendulum model is imperfect. We opt for LQR over anti-swing planning methods like [18] to avoid the need to follow a planned trajectory, which would limit reactivity and increase complexity.

Furthermore, we integrate the hanging tray into an interactive robot waiter demonstration, inspired by previous robot waiters like Alfred [19]. We use a CNN to detect people with a raised hand and use visual servoing to steer toward them. Visual servoing—that is, closed-loop motion control based on visual input—has a long history [20], and gesture recognition for human-robot interaction has also been extensively studied [21], [22], but fewer works have combined the two. In [23], a mobile robot uses visual servoing to track and follow a person while also identifying gestures made by the person to trigger

a behavior change, such as to start or stop a task. Similarly, [24] trains a classifier to identify a particular person in a camera feed given a reference image of that person, which allows a mobile robot to dynamically track an individual around the environment and deliver items to them, but does not use gesture recognition. In [25], a CNN is trained to identify hand gestures. A fixed-based manipulator then uses visual servoing to track the gesturing hand with its EE. Likewise, in [26], a custom neural network is trained to recognize hand gestures, which are used to command both a manipulator and a mobile robot with manipulation targets and movement commands, respectively. However, our work is the first time gesture-based visual servoing has been used explicitly for the waiter’s problem; that is, visual servoing is used to steer a mobile robot toward a gesturing person while bringing them an object transported on a tray.

## III. SYSTEM MODELS

Here we develop models of the 3D pendulum and combined tray-object system, which we use for subsequent control design and numerical experiments. We denote the  $n \times n$  identity matrix as  $\mathbf{1}_n$ , the set of  $n \times n$  symmetric positive semidefinite matrices as  $\mathbb{S}_+^n$ , and the set of  $n \times n$  symmetric positive definite matrices as  $\mathbb{S}_{++}^n$ .

### A. Pendulum Model

The dynamics of a rigid body can be expressed using the body-frame Newton-Euler equations:

$$\mathbf{w} = \mathbf{M}\dot{\boldsymbol{\xi}} - \text{ad}(\boldsymbol{\xi})^T \mathbf{M}\boldsymbol{\xi},$$

where  $\mathbf{w} = [\boldsymbol{\tau}^T, \mathbf{f}^T]^T$  is the applied wrench with torque  $\boldsymbol{\tau} \in \mathbb{R}^3$  and force  $\mathbf{f} \in \mathbb{R}^3$ ,  $\mathbf{M} \in \mathbb{S}_+^6$  is the body’s spatial mass matrix,  $\boldsymbol{\xi} = [\boldsymbol{\omega}^T, \mathbf{v}^T]^T$  is the spatial velocity with angular component  $\boldsymbol{\omega} \in \mathbb{R}^3$  and linear component  $\mathbf{v} \in \mathbb{R}^3$ , and

$$\text{ad}(\boldsymbol{\xi}) \triangleq \begin{bmatrix} \boldsymbol{\omega}^\times & \mathbf{0} \\ \mathbf{v}^\times & \boldsymbol{\omega}^\times \end{bmatrix}$$

is the adjoint of  $\boldsymbol{\xi}$  with  $(\cdot)^\times$  forming a skew-symmetric matrix such that  $\mathbf{a}^\times \mathbf{b} = \mathbf{a} \times \mathbf{b}$  for any  $\mathbf{a}, \mathbf{b} \in \mathbb{R}^3$ . The spatial mass matrix is defined as

$$\mathbf{M} = \begin{bmatrix} \mathbf{I} & \mathbf{h}^\times \\ -\mathbf{h}^\times & m\mathbf{1}_3 \end{bmatrix},$$

where  $\mathbf{I} \in \mathbb{S}_+^3$  is the inertia matrix and  $\mathbf{h} = m\mathbf{c}$  is the first moment of mass with mass  $m > 0$  and center of mass (CoM)  $\mathbf{c} \in \mathbb{R}^3$ .

A 3D pendulum [27] is a rigid body that is constrained to rotate about a pivot point  $O$ ; that is, its position is fixed but it retains all three rotational degrees of freedom. Taking  $O$  as the origin of the body frame and assuming the only external force is gravity, the dynamics simplify to Euler’s equation:

$$\mathbf{h}^\times \mathbf{C}^T \mathbf{g} = \mathbf{I}\dot{\boldsymbol{\omega}} + \boldsymbol{\omega}^\times \mathbf{I}\boldsymbol{\omega}, \quad (1)$$

where  $\mathbf{C} \in SO(3)$  is the pendulum’s orientation and  $\mathbf{g} \in \mathbb{R}^3$  is the gravitational acceleration expressed in the global inertial

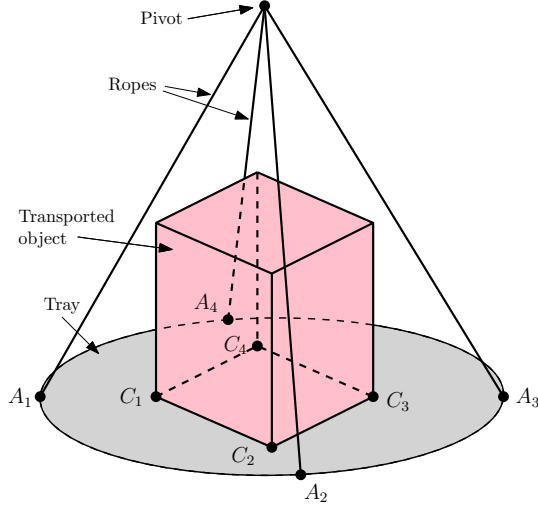


Figure 2: A hanging tray (gray) supporting an object (red). The tray is suspended from a pivot point by ropes attached to the anchor points  $A_1$ – $A_4$ . We model contact between the object and tray using a discrete set of contact points  $C_1$ – $C_4$  at the vertices of the contact area.

frame. The orientation  $C$  and body-frame angular velocity  $\omega$  are related by the kinematics equation  $\dot{C} = C\omega^\times$ .

In our case, the pivot point is attached to the robot's EE, which is itself moving. Let  $u \in \mathbb{R}^3$  be the acceleration of the pivot point in the global frame. Then the dynamics (1) are augmented to

$$h^\times C^T (g - u) = I\dot{\omega} + \omega^\times I\omega. \quad (2)$$

If we assume  $c^T \omega = 0$  and that all mass is concentrated at  $c$  (such that  $I = -mc^\times c^\times$ ), then the system is known as a spherical or 2D pendulum, and the dynamics (2) simplify to

$$c^\times C^T (g - u) = \ell^2 \dot{\omega}, \quad (3)$$

where  $\ell = \|c\|_2$ .

### B. Tray-Object Model

Suppose that the hanging tray is supporting an object, which we assume is a rigid body, as shown in Fig. 2. Let  $M_o$  be the object's spatial mass matrix and let  $M_t$  be the tray's spatial mass matrix. Let us assume that there is no relative motion between the object and tray, so that they share the same orientation  $C$  and spatial velocity  $\xi$ . Given a commanded EE acceleration  $u \in \mathbb{R}^3$ , we can solve for their shared spatial acceleration using (2) and the kinematic relationship  $u = d(Cv)/dt$  to obtain

$$\dot{\xi} = \begin{bmatrix} \dot{\omega} \\ \dot{v} \end{bmatrix} = \begin{bmatrix} \tilde{I}^{-1}(\tilde{h}^\times C^T (g - u) - \omega^\times \tilde{I}\omega) \\ C^T u - \omega^\times v \end{bmatrix},$$

where

$$\tilde{M} = \begin{bmatrix} \tilde{I} & \tilde{h}^\times \\ -\tilde{h}^\times & \tilde{m}\mathbf{1}_3 \end{bmatrix} = M_t + M_o$$

is the spatial mass matrix of the combined system.

We assume that the object and tray interact through a set of  $n_c$  contact forces  $\{f_{c_i}\}_{i=1}^{n_c}$ , located at points  $\{r_{c_i}\}_{i=1}^{n_c}$ . To

ensure that our assumption that there is no relative motion between the two bodies holds, we must be able to find a set of feasible contact forces; that is, the contact forces must lie within their Coulomb friction cones, defined by

$$\sigma_{c_i}(f_{c_i}) \triangleq \mu_{c_i} \hat{n}_{c_i}^T f_{c_i} - \|\hat{n}_{c_i}^\times \hat{n}_{c_i}^\times f_{c_i}\|_2 \geq 0, \quad (4)$$

where  $\mu_{c_i} \geq 0$  is the friction coefficient and  $\hat{n}_{c_i} \in \mathbb{R}^3$  is the unit-length contact normal. In our numerical experiments, it will be useful to relax (4) to

$$\sigma(f_{c_i}) \geq s \quad (5)$$

with slack variable  $s \in \mathbb{R}$ , where  $s \geq 0$  indicates that the original constraint (4) is feasible.

Furthermore, we suspend the tray from the pivot point on the EE using  $n_a$  ropes attached to the tray at anchor points  $\{r_{a_i}\}_{i=1}^{n_a}$ , so we also need to constrain the tensile forces  $f_{a_i} \in \mathbb{R}$ ,  $i = 1, \dots, n_a$ , along each rope to be non-negative. That is, we need to find contact and tensile forces that satisfy the following system of constraints:

$$\begin{aligned} w_a - w_c + m_t G(c_t) C^T g &= M_t \dot{\xi} - \text{ad}(\xi)^T M_t \xi, \\ w_c + m_o G(c_o) C^T g &= M_o \dot{\xi} - \text{ad}(\xi)^T M_o \xi, \\ \sigma(f_{c_i}) &\geq s, \quad i = 1, \dots, n_c, \\ f_{a_i} &\geq 0, \quad i = 1, \dots, n_a, \end{aligned} \quad (6)$$

where the first two lines are the Newton-Euler equations for the tray and object, respectively, with tensile and contact wrenches

$$w_a = \sum_i^{n_a} f_{a_i} G(r_{a_i}) r_{a_i}, \quad w_c = \sum_i^{n_c} G(r_{c_i}) f_{c_i},$$

where  $G(p) = [-p^\times, \mathbf{1}_3]^T$  for any  $p \in \mathbb{R}^3$ . To facilitate comparison in our numerical experiments, we will determine the feasible contact forces by solving the following convex optimization problem:<sup>1</sup>

$$\begin{aligned} s^* &= \text{maximize } s \\ &\text{subject to } (6), \end{aligned} \quad (7)$$

which finds the contact forces with the largest friction constraint margin. If  $s^* \geq 0$ , then all of the contact forces are feasible under the Coulomb model (4). In contrast,  $s^* < 0$  implies that no feasible contact forces can be found to resist the object's motion, at which point we stop the simulation. The controller itself does not depend on the contact forces, but they must be computed while *simulating* the system to determine if the object moves relative to the tray.

## IV. SWING ATTENUATION

After the robot's EE reaches a desired location and stops, the tray will continue to swing until all of its energy is lost to friction and damping. We would like to speed up this process and rapidly bring the tray to rest, to facilitate a person interacting with objects on it. To do so, we design

<sup>1</sup>Using the friction cone constraint (4) or its relaxed version (5) results in a second-order cone program. It is also common to linearize (4), making (7) a linear program.

a linear-quadratic regulator (LQR) using the simplified 2D pendulum model (3) linearized about the hanging equilibrium point, which is a similar approach to [17] except that we also introduce an integral term to eliminate steady-state pivot position error. It is convenient to parameterize (3) with a unit vector  $\delta \in \mathbb{R}^3$  pointing from the pivot position  $r \in \mathbb{R}^3$  toward the pendulum’s CoM, rather than the rotation matrix  $C$ . The state is  $x = [\gamma^T, r^T, \delta^T, \dot{r}^T, \dot{\delta}^T]^T \in \mathbb{R}^{15}$ , where  $\gamma \in \mathbb{R}^3$  is the time integral of  $r$  (that is,  $\gamma$  is the pivot’s *absement*), with all quantities expressed in the global frame. We found that the addition of an integral term is necessary to eliminate steady-state error in the presence of model errors like an inaccurate pendulum CoM, as we will demonstrate in Sec. VI. The nonlinear equations of motion are

$$\dot{x} = f(x, u) = \begin{bmatrix} r \\ \dot{r} \\ \dot{\delta} \\ u \\ -\|\dot{\delta}\|^2 \delta - \delta \times \delta \times (g - u) / \ell \end{bmatrix},$$

which we linearize by computing the Jacobians  $A \triangleq \partial f / \partial x$  and  $B \triangleq \partial f / \partial u$  about the hanging equilibrium. However, the  $z$ -component of  $\delta$  is not controllable in this linearized system and our mobile robot cannot change the  $z$ -component of  $r$ . We therefore use the reduced state  $x' \in \mathbb{R}^{10}$  and input  $u' \in \mathbb{R}^2$ , which drop all  $z$ -components, and corresponding reduced matrices  $A' \in \mathbb{R}^{10 \times 10}$  and  $B' \in \mathbb{R}^{10 \times 2}$ . This gives us the linearized system  $\dot{x}' = A'x' + B'u'$ , for which we use LQR to obtain the linear feedback law

$$u' = -K(x' - x'_d), \quad (8)$$

where  $x_d = [\gamma_d^T, r_d^T, \mathbf{0}^T, \mathbf{0}^T]^T$  with  $r_d$  the desired pivot position and  $\gamma_d$  its integral. The gain matrix is  $K = R^{-1}B'^T P$ , where  $P$  is obtained by solving the continuous-time algebraic Riccati equation

$$A'^T P + P A' - P B' R^{-1} B'^T P + Q = 0$$

given tunable gain matrices  $Q \in \mathbb{S}_{++}^{10}$  and  $R \in \mathbb{S}_{++}^2$ . In all experiments we use  $Q = \mathbf{1}_{10}$  and  $R = 0.1\mathbf{1}_2$ .

## V. INTERACTIVE ROBOT WAITER

We now describe how to integrate the hanging tray into an interactive robot waiter system, where the use of a hanging tray is appealing because it allows the robot to move freely without worrying about the transported objects falling. An RGB-D camera is used to observe the scene and detect humans to serve.

### A. State Machine

The robot’s behavior is dictated by a simple state machine with four states, depicted in Fig. 3. They are:

- **HOME**: the robot starts at a known home position in the room. If a person within view of the camera raises their hand, the robot starts to **FOLLOW** the person.
- **FOLLOW**: the robot moves forward while using visual servoing to steer toward the person with their hand up. If

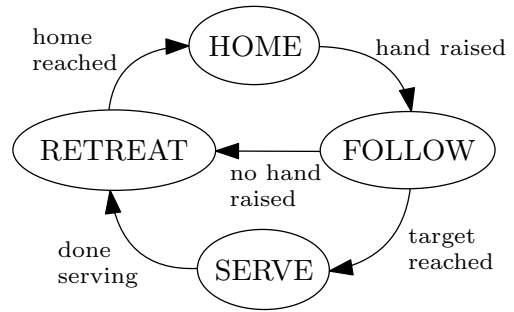


Figure 3: State machine for our interactive robot waiter demonstration with four states. The robot waits at the HOME position until a person raises their hand. It then **FOLLOWS** them using visual servoing until it arrives and **SERVES** them or the hand is lowered; in either case, the robot then **RETREATS** back to the home position until another hand is raised.

the person puts their hand down and there are no other people with hands up, then the robot **RETREATS**. If the robot reaches the target person, then it **SERVES** them.

- **SERVE**: once the robot is within a threshold distance to the target person (as measured by the depth camera), the robot stops, attenuates the swinging of the tray using the control law (8), and then waits a pre-defined amount of time for the person to interact with the tray. Once done, the robot **RETREATS**.
- **RETREAT**: the robot moves back to the home position. If a person with their hand up is observed, the robot switches to **FOLLOWING** them.

Acceleration limits are enforced whenever the velocity changes between states. The hand gesture detection and visual servoing procedures are described in more detail below.

### B. Gesture Recognition and Visual Servoing

The scene is observed using an RGB-D camera mounted at the EE. We use a customized YOLOv11 model [28] to obtain segmentation masks of people with a hand raised. We use the COCO-Pose dataset [29], which provides labelled human segmentation masks and pose keypoints. The keypoints define a skeleton of 17 points, including the nose, each eye, each ear, and each wrist. We process the dataset so that each human segmentation mask is labelled either *hand-up* or *hand-down*, using the following procedure. For each human instance in each image, we compute the head height  $h_{\text{head}}$  (in image coordinates) as the mean value of the height of the nose, eye, and ear keypoints, omitting any of these keypoints that are not visible. The instance is classified as *hand-up* if either wrist keypoint is above  $h_{\text{head}}$ , and *hand-down* otherwise. We then re-train the YOLOv11 segmentation model on this dataset to predict (only) these two classes of segmentation mask. The upshot is that we obtain a model that robustly segments people with a raised hand from images.

Given an image containing a person with a raised hand and that person’s segmentation mask, we compute a horizontal target  $\alpha_x$  for the robot to steer toward using visual servoing.<sup>2</sup> In

<sup>2</sup>Since we are only controlling the mobile base, we only care about a horizontal target. If the arm were being used, it could raise the EE up and down to also align with a vertical target.

particular, we take  $\alpha_x$  to be the median of the horizontal values of the segmentation mask, normalized to the interval  $[-1, 1]$  with the origin at the center of the image. The robot moves forward with linear velocity  $v = \bar{v}(1 - |\alpha_x|)$  and angular velocity  $\omega = k_\omega \alpha_x$ , where  $\bar{v}, k_\omega > 0$  are tunable parameters. The velocity  $v$  moves the robot toward the target but is reduced as  $|\alpha_x|$  increases, while  $\omega$  rotates the robot to reduce  $|\alpha_x|$  (i.e., to center the target in the camera’s view). We compute the median depth over the segmentation mask to determine the current distance to the target person.

## VI. NUMERICAL EXPERIMENTS

We now present numerical simulations to provide insight into how the hanging tray and object system described by (6) behaves. We simulate the system forward in time from initial state  $(\mathbf{r}_0, \mathbf{C}_0, \boldsymbol{\xi}_0) = (\mathbf{0}, \mathbf{1}_3, \mathbf{0})$ . Given the pivot acceleration  $\mathbf{u}_k$  at each simulation timestep  $k$ , we solve (7) to look for feasible forces and then use the semi-implicit Lie-Euler method to integrate the system to timestep  $k + 1$ :

$$\begin{aligned} \dot{\mathbf{r}}_{k+1} &= \dot{\mathbf{r}}_k + \Delta t \mathbf{u}_k, & \boldsymbol{\omega}_{k+1} &= \boldsymbol{\omega}_k + \Delta t \dot{\boldsymbol{\omega}}_{k+1}, \\ \mathbf{r}_{k+1} &= \mathbf{r}_k + \Delta t \dot{\mathbf{r}}_{k+1}, & \mathbf{C}_{k+1} &= \mathbf{C}_k \exp(\Delta t \boldsymbol{\omega}_{k+1}^\times), \end{aligned}$$

where  $\exp(\cdot)$  is the matrix exponential and  $\Delta t = 10$  ms is the integration timestep. This approach ensures that  $\mathbf{C}$  stays on the  $SO(3)$  manifold. We use the Clarabel solver [30] via CVXPY [31] to solve (7).

### A. Robustness to Parameter Variation

In the theoretical limiting case when both the tray and object are point masses located at the same position, no shear forces are applied to the object no matter the pivot acceleration, and no sliding occurs. While not physically realizable, this case agrees with the intuition that an object with its mass concentrated closer to the tray is less likely to move. Here we explore how different parameters of the system affect its ability to resist movement of the object with respect to the tray.

We model the tray as a thin disk with radius 20 cm and thickness 1 mm transporting a box with side lengths  $10 \text{ cm} \times 10 \text{ cm} \times h$  placed directly over the tray’s center point, where  $h > 0$  is the height of the box, similar to the setup in Fig. 2. Both the tray and object have mass 0.5 kg and a uniform mass distribution. We use  $n_c = 4$  contact points between the tray and object, located at the contact area’s vertices, with friction coefficient  $\mu = 0.1$  (i.e., fairly slippery; indeed, lower and thus more difficult than the measured values used in the real-world experiments below). The tray is suspended from  $n_a = 4$  evenly spaced ropes such that it hangs at a length  $\ell$  below the pivot point. Gravitational acceleration is  $\mathbf{g} = [0, 0, -9.81]^T \text{ m/s}^2$ . We apply a horizontal acceleration corresponding to a trapezoidal velocity profile to the pivot point. As shown in Fig. 4, the trajectory consists of a constant acceleration  $a$  for 2 s, a constant velocity for an additional 2 s, and another constant acceleration of  $-a$  for a final 2 s.

We vary the values of  $a$ ,  $h$  and  $\ell$  and compare the friction constraint satisfaction between a hanging tray and a “static” tray that is rigidly attached to the pivot point (i.e., the EE).

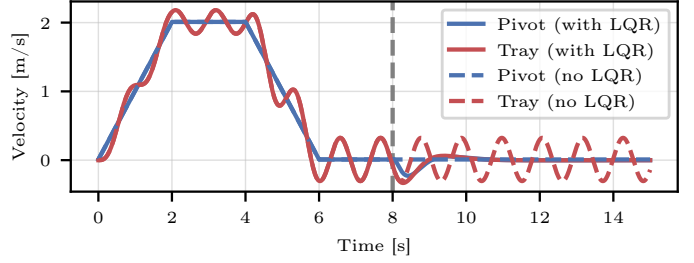


Figure 4: Simulated pivot and tray velocities, with and without LQR-based swing attenuation. When the LQR controller is activated at  $t = 8$  s (dashed vertical line), it quickly damps out the tray’s velocity by briefly moving the pivot. Without it, the tray simply keeps swinging.

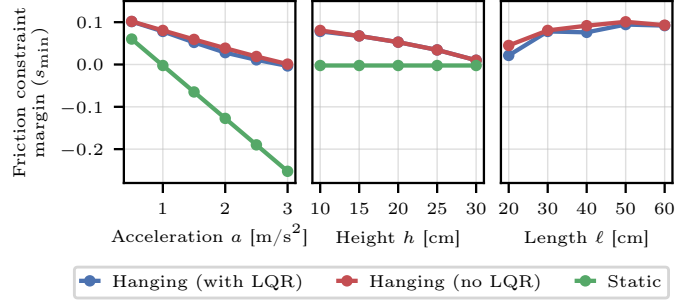


Figure 5: Friction constraint margin, defined as the minimum value  $s_{\min}$  of  $s^*$  obtained along the trajectory by solving (7) at each simulation timestep. When  $s^* < 0$ , no feasible set of friction forces exists, and the constraint is violated. The hanging tray results in higher constraint margins across a range of pivot accelerations and object heights compared to the static tray. Increasing the length of the pendulum also typically increases the constraint margin.

For the hanging tray, we also compare the effect of swing attenuation using the LQR control law (8). When LQR is used, we wait 2 s after the end of the trajectory and then apply (8) for 8 s. We limit the magnitude of the pivot’s acceleration input computed from (8) to no more than  $1 \text{ m/s}^2$ . For each parameter of interest, we vary it while the others are fixed at the nominal values of  $a = 1 \text{ m/s}^2$ ,  $h = 10 \text{ cm}$ , and  $\ell = 30 \text{ cm}$ . As can be seen from the results shown in Fig. 5, the hanging tray can handle much higher accelerations without violating the friction constraints. The static tray results in constraint violation for any acceleration  $a > \mu \|\mathbf{g}\| = 0.981 \text{ m/s}^2$ , but the hanging tray only starts to violate the constraints at  $a = 3 \text{ m/s}^2$ . The hanging tray is also robust to different object heights  $h$ : the constraint margin decreases as height increases, but is still positive at  $h = 30 \text{ cm}$  with the nominal acceleration  $a = 1 \text{ m/s}^2$ . In contrast, the constraint violation with the static tray is independent of object height, and even at  $a = 1 \text{ m/s}^2$  the constraints are violated. Finally, we see that increasing the length  $\ell$  of the pendulum typically increases the constraint margin, while swing attenuation has a minimal impact on it.

### B. Swing Attenuation

Let us now explore the behavior of swing attenuation in more detail. Fig. 4 shows the velocities of the hanging tray and pivot point using the nominal parameter values of  $a = 1 \text{ m/s}^2$ ,  $h = 10 \text{ cm}$ , and  $\ell = 30 \text{ cm}$ , with and without LQR-based swing attenuation. The trajectories are the same until  $t = 8$  s,

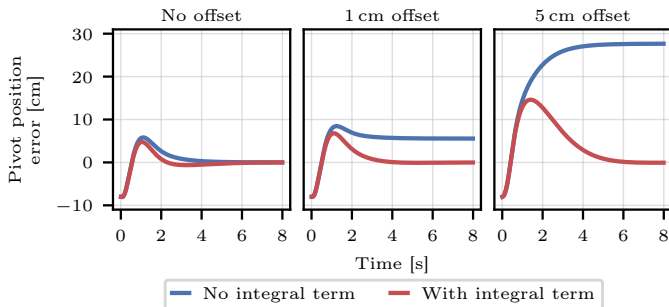


Figure 6: Effect of including the integral term  $\gamma$  in the LQR-based swing attenuation controller on the pivot position error. When the transported object is offset from the center of the tray, such that the CoM of the combined system is no longer directly between the pivot and tray CoM, then substantial steady-state error occurs unless  $\gamma$  is used.

when the LQR-based controller (8) is activated. With swing attenuation, the pivot moves to quickly damp out the tray’s velocity. Without it, the tray simply keeps swinging.

Next, we examine the effect of the integral term  $\gamma$  we included in the LQR model. The model assumes that the CoM of the combined tray-object system is located along the line between the pivot point and the tray’s CoM. However, this assumption is easily violated if the object is placed such that its CoM is horizontally offset from that of the tray. This offset results in steady-state error in the pivot position unless  $\gamma$  is included in the LQR-based controller. We apply the same trapezoidal trajectory to the pivot as in the previous subsection (again, using the nominal parameter values) while varying the  $x$ -offset of the object with respect to the tray and we compare the results with and without the integral term; the results are shown in Fig. 6. When there is no offset, including  $\gamma$  makes little difference. However, we see substantial steady-state error in the pivot position when there is an offset unless  $\gamma$  is used. Indeed, with an offset of 5 cm, the resulting steady-state error without  $\gamma$  is over 25 cm; that is, the pivot ends up over 25 cm from where we want it to be, which is not acceptable when positioning the tray in a particular location to allow humans to interact with it.

### C. A Failure Case

Finally, let us consider an interesting failure mode of the hanging tray-object system, which stems from the fact that it stores energy. This means that it is possible to design an input pivot acceleration signal that pumps energy into the system until the transported object slides and falls off the tray. Notably, this can be achieved while keeping the EE acceleration below what is required to make the object slide on a static tray. Let  $\dot{\mathbf{r}}_t$  be the velocity of the tray’s CoM in the global frame. Suppose the tray is moving, and we apply the control law

$$\mathbf{u} = \begin{cases} -a(\dot{\mathbf{r}}_t - \dot{\mathbf{r}})/\|\dot{\mathbf{r}}_t - \dot{\mathbf{r}}\|_2 & \text{if } \|\dot{\mathbf{r}}_t - \dot{\mathbf{r}}\|_2 > 0, \\ \mathbf{0} & \text{otherwise,} \end{cases} \quad (9)$$

which applies an acceleration  $a$  in the opposite direction of the tray’s velocity relative to the pivot point. This is similar to the control law designed in [32] to swing up a pendulum.

Table I: Measured friction coefficients between objects and trays.

| Tray    | Object |        |
|---------|--------|--------|
|         | Cup    | Bottle |
| Static  | 0.34   | 0.22   |
| Hanging | 0.26   | 0.19   |

To demonstrate this failure case, we perform a simple simulation where the pivot point accelerates horizontally at  $a = 0.5 \text{ m/s}^2$  for 2s, then switches to the control law (9). With  $\mu = 0.1$ , the acceleration is too low for any sliding to occur with a static tray. However, the hanging tray system eventually fails to find feasible contact forces at  $t = 4.69 \text{ s}$ , indicating that the transported object would start to move with respect to the tray. This failure mode is adversarial in nature, because one has to apply a fairly specific input signal to achieve it. However, it demonstrates how the hanging tray system is more nuanced than a static tray, which only requires hard acceleration limits to prevent slipping.

## VII. HARDWARE EXPERIMENTS

Having developed some intuition with numerical experiments, we now validate our proposed approach with experiments on the real mobile manipulator shown in Fig. 1, which consists of a 3-DOF Ridgeback omnidirectional mobile base and a 6-DOF UR10 manipulator. However, since one of the key motivations for using a hanging tray is that the EE does not need to be actuated to prevent objects from sliding, we do not move the UR10 arm at all in any experiments; all motion is achieved with the mobile base alone. The base and hanging tray are localized using a Vicon motion capture system; the tray’s velocity is obtained using numerical differentiation. The robot is velocity-controlled, so the acceleration input (8) for attenuating the tray’s swinging is integrated in time to obtain velocity commands. All experiments are run on a standard laptop with 16 GB of RAM and a NVIDIA Quadro M2200 GPU. We run our control loop at 25 Hz, which is the frequency at which the base accepts commands. The reader is encouraged to watch the video of the experiments at <http://tiny.cc/visual-server>.

### A. Pendular Transport

Let us compare the behavior of the hanging tray and static tray in the real world. The static tray is held rigidly by the robot’s gripper and the hanging tray that is suspended from the EE using ropes, as shown in Fig. 9.

1) *Rigid Objects*: We begin with experiments transporting two different (approximately) rigid objects: a short cup and a taller water bottle, also shown in Fig. 9. The cup contains two bean bags (to simulate being filled without risking a spill) and the bottle is filled with water (but is securely sealed). The cup is 8 cm tall and weighs 239 g. The bottle is 19 cm tall and weighs 514 g. The two trays are made of different materials, but we cover each with paper to provide similar surfaces. Despite this, the measured friction coefficients (given in Table I) between the objects and the hanging tray are slightly

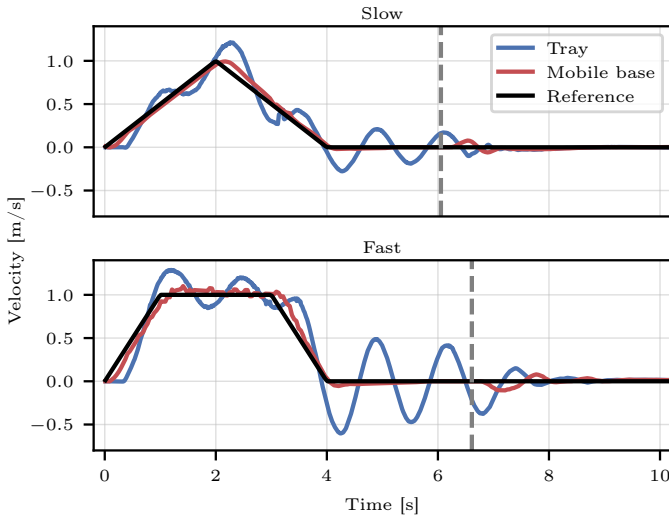


Figure 7: Velocity response of the mobile base and hanging tray for the slow and fast motion profiles. The vertical dashed line is the time at which swing attenuation is started, damping out the tray’s velocity within a few seconds. The velocities are obtained by numerically differentiating the measured positions from the motion capture system and applying a small moving average filter.

lower than with the static tray. However, this makes relative motion *more* likely with the proposed hanging tray, making the comparison to the baseline static tray even stronger.

To test the ability of each tray to transport each object, we command the base to move in one direction with a particular motion profile and measure the distance the object moves from its initial position on the tray using motion capture. Two trapezoidal motion profiles are used: *slow* and *fast*. Starting from rest, the *slow* trajectory has a constant acceleration of  $0.5 \text{ m/s}^2$  for 2s, reaching a maximum velocity of 1 m/s, before immediately accelerating at  $-0.5 \text{ m/s}^2$  for a further 2s and returning to rest at  $t = 4 \text{ s}$ . The *fast* trajectory accelerates from rest at  $1 \text{ m/s}^2$  for 1s to reach the same maximum velocity of 1 m/s. It holds this velocity constant for 2s before accelerating at  $-1 \text{ m/s}^2$  for a further 1s and returning to rest at  $t = 4 \text{ s}$ . Both motion profiles are shown in Fig. 7, along with the actual velocities of the base and hanging tray from one of the experiments. When using the hanging tray, we wait 1s after the robot has come back to rest before using the LQR-based controller (8) to attenuate the swinging of the tray; Fig. 7 shows how the oscillations of the tray are quickly damped out by briefly moving the mobile base.

For each combination of transported object (cup or bottle), tray (static or hanging), and motion profile (slow or fast), we perform three runs, for a total of 24 experiments. The maximum object error across any of the three runs for each combination is plotted in Fig. 8. The hanging tray resulted in almost no sliding of either object for both motion profiles, with at most 3 mm of error. In contrast, the static tray results in over 20 mm of error in every case. While the commanded accelerations should theoretically be low enough to avoid sliding on the static tray, unmodelled effects and vibrations result in object motion that the hanging tray avoids.

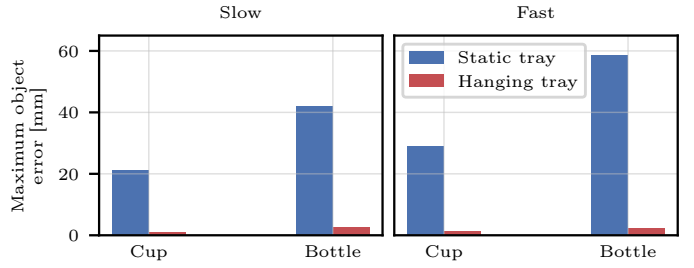


Figure 8: Maximum object error across different combinations of trajectory profile, object, and tray type. The error is the maximum distance that the object moved from its initial position relative to the tray; each value is the average across three trials, with 24 experiments in total. The hanging tray results in substantially lower error than the static tray, because its swinging naturally reduces the shear forces acting on the objects.

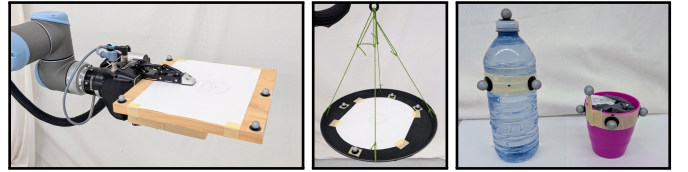


Figure 9: From left: The static tray, the hanging tray, and the two objects used in experiments: a water bottle and a cup.

2) *Liquid Handling*: Previous work [13] on pendular motion was focused on transporting liquids while minimizing slosh and spillage, so we also perform an experiment to assess the hanging tray’s ability to transport liquid without spilling. To avoid uncontrolled spills, we use a cup rigidly set within a larger container that is in turn rigidly attached to the tray (see Fig. 10). For each experiment, the cup is filled with 200 ml of water colored with red food dye, which is free to slosh out of the cup (but any spill is captured inside the larger container). As shown in Fig. 10, the hanging tray results in no spill, while a considerable amount of liquid sloshed out of the cup with the static tray.

### B. Interactive Robot Waiter

As a final experiment, we present a demonstration of our full interactive waiter using visual servoing, as described in Sec. V, with parameters  $\bar{v} = 0.3 \text{ m/s}$  and  $k_{\omega} = 0.5$ . The robot is equipped with the hanging tray carrying four cups while two people are sitting nearby. An Orbbec Femto Bolt RGB-D camera attached to the EE is used to observe the scene. Each person raises their hand in turn to summon the robot and take a cup from the tray without leaving their seats. Some salient still images of the experiment are shown in Fig. 11, but we encourage the reader to watch the accompanying video to see the full demonstration in action.

## VIII. CONCLUSION

We presented an approach for robotic nonprehensile object transportation using a hanging tray, the dynamics of which naturally reduce the shear forces acting on the transported objects and prevent them from sliding, without requiring an actuated robot arm. We demonstrated this approach using rigid objects, liquid, and in an interactive robot waiter experiment.



Figure 10: Liquid handling experiments. The blue cup is rigidly set in the center of the larger plastic container and filled with 200 ml of water colored red with food dye. The water is free to slosh out of the cup but will be caught in the larger container. The container is rigidly attached to the tray during experiments. *From left:* Top view before experiments; after executing the fast trajectory with the hanging tray; after executing it with the static tray. No liquid spilled from the cup when using the hanging tray, but a considerable amount was spilled with the static tray (the pink spill can be seen collected in the bottom of the larger container).

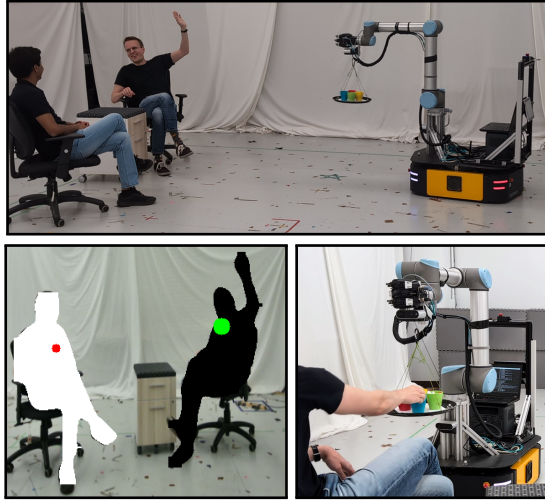


Figure 11: *Top:* A person is raising his hand to indicate that he wants to be served by the robot and the robot is moving toward him. *Bottom left:* The view from the robot's camera: the person with his hand up is segmented in black; the person with his hand down is segmented in white. The large green dot is the current target to steer toward using visual servoing. *Bottom right:* The robot has reached the person and waits while a cup is taken from the tray. The full demonstration can be seen at <http://tiny.cc/visual-serveror>.

## REFERENCES

- [1] F. G. Flores and A. Kecskeméthy, "Time-optimal path planning for the general waiter motion problem," in *Advances in Mechanisms, Robotics and Design Education and Research*, 2013, pp. 189–203.
- [2] K. M. Lynch, "Nonprehensile robotic manipulation: Controllability and planning," Ph.D., Carnegie Mellon University, 1996.
- [3] A. Heins and A. P. Schoellig, "Force push: Robust single-point pushing with force feedback," *IEEE Robotics and Automation Letters*, vol. 9, no. 8, pp. 6856–6863, 2024.
- [4] F. Ruggiero, V. Lippiello, and B. Siciliano, "Nonprehensile dynamic manipulation: A survey," *IEEE Robotics and Automation Letters*, vol. 3, no. 3, pp. 1711–1718, 2018.
- [5] Q.-C. Pham, S. Caron, P. Lertkultanon, and Y. Nakamura, "Admissible velocity propagation: Beyond quasi-static path planning for high-dimensional robots," *Int. J. Robotics Research*, vol. 36, no. 1, pp. 44–67, 2017.
- [6] A. Dang and I. Ebert-Uphoff, "Active acceleration compensation for transport vehicles carrying delicate objects," *IEEE Trans. Robotics*, vol. 20, no. 5, pp. 830–839, 2004.
- [7] C. Zhou, M. Lei, L. Zhao, Z. Wang, and Y. Zheng, "TOPP-MPC-based dual-arm dynamic collaborative manipulation for multi-object nonprehensile transportation," in *Proc. IEEE Int. Conf. Robotics and Automation*, 2022, pp. 999–1005.
- [8] H. Gattringer, A. Müller, S. Weitzhofer, and M. Schörgenhumer, "Point to point time optimal handling of unmounted rigid objects and liquid-filled containers," *Mechanism and Machine Theory*, vol. 184, p. 105286, 2023.

- [9] Z. Brei, J. Michaux, B. Zhang, P. Holmes, and R. Vasudevan, "Serving time: Real-time, safe motion planning and control for manipulation of unsecured objects," *IEEE Robotics and Automation Letters*, vol. 9, no. 3, pp. 2383–2390, 2024.
- [10] M. Selvaggio, A. Garg, F. Ruggiero, G. Oriolo, and B. Siciliano, "Non-prehensile object transportation via model predictive non-sliding manipulation control," *IEEE Trans. Control Systems Technology*, pp. 1–14, 2023.
- [11] A. Heins and A. P. Schoellig, "Keep it upright: Model predictive control for nonprehensile object transportation with obstacle avoidance on a mobile manipulator," *IEEE Robotics and Automation Letters*, vol. 8, no. 12, pp. 7986–7993, 2023.
- [12] L. Moriello, L. Biagiotti, C. Melchiorri, and A. Paoli, "Manipulating liquids with robots: A sloshing-free solution," *Control Engineering Practice*, vol. 78, pp. 129–141, 2018.
- [13] R. I. C. Muchacho, R. Laha, L. F. C. Figueredo, and S. Haddadin, "A solution to slosh-free robot trajectory optimization," in *Proc. IEEE/RSJ Int. Conf. Intelligent Robots and Systems*, 2022, pp. 223–230.
- [14] M. Selvaggio, J. Cacace, C. Pacchierotti, F. Ruggiero, and P. R. Giordano, "A shared-control teleoperation architecture for nonprehensile object transportation," *IEEE Trans. Robotics*, vol. 38, no. 1, pp. 569–583, 2022.
- [15] R. Subburaman, M. Selvaggio, and F. Ruggiero, "A non-prehensile object transportation framework with adaptive tilting based on quadratic programming," *IEEE Robotics and Automation Letters*, pp. 1–8, 2023.
- [16] J. Millstein, "Hanging tray for single open beverage," 2012, US Patent 8,220,655.
- [17] W. August, J. Ren, S. Notheis, T. Haase, B. Hein, and H. Woern, "3D pendulum swinging control by an industrial robot manipulator," in *Proc. Int. Symp. Robotics*, 2010, pp. 1–7.
- [18] S. J. Chen, B. Hein, and H. Worn, "Swing attenuation of suspended objects transported by robot manipulator using acceleration compensation," in *Proc. IEEE/RSJ Int. Conf. Intelligent Robots and Systems*, 2007, pp. 2919–2924.
- [19] B. A. Maxwell *et al.*, "Alfred: The robot waiter who remembers you," in *Proc. AAAI Workshop on Robotics*, 1999, pp. 1–12.
- [20] S. Hutchinson, G. Hager, and P. Corke, "A tutorial on visual servo control," *IEEE Trans. Robotics and Automation*, vol. 12, no. 5, pp. 651–670, 1996.
- [21] H. Liu and L. Wang, "Gesture recognition for human-robot collaboration: A review," *Int. J. Industrial Ergonomics*, vol. 68, pp. 355–367, 2018.
- [22] J. Qi, L. Ma, Z. Cui, and Y. Yu, "Computer vision-based hand gesture recognition for human-robot interaction: A review," *Complex & Intelligent Systems*, vol. 10, no. 1, pp. 1581–1606, 2024.
- [23] S. Waldherr, R. Romero, and S. Thrun, "A gesture based interface for human-robot interaction," *Autonomous Robots*, vol. 9, no. 2, pp. 151–173, 2000.
- [24] G. Sawadwuthikul, T. Tothong, T. Lodkaew, P. Soisudararat, S. Nutanong, P. Manoonpong, and N. Dilokthanakul, "Visual goal human-robot communication framework with few-shot learning: A case study in robot waiter system," *IEEE Trans. Industrial Informatics*, vol. 18, no. 3, pp. 1883–1891, 2022.
- [25] A. Al-Shanoon, H. Lang, and Y. Wang, "Vision-based hand gesture recognition with deep machine learning for visual servoing," in *Proc. ASME Int. Design Engineering Technical Conf. and Computers and Information in Engineering Conf.*, 2018.
- [26] H. Zhang, L. Zhang, X. Chen, and F. Wang, "A visual servo human-robot interaction method based on unidirectional adaptive temporal interaction," in *Proc. IEEE Int. Conf. Robotics and Biomimetics*, 2024, pp. 1769–1774.
- [27] J. Shen, A. Sanyal, N. Chaturvedi, D. Bernstein, and H. McClamroch, "Dynamics and control of a 3D pendulum," in *Proc. IEEE Conf. Decision and Control*, 2004, pp. 323–328.
- [28] G. Jocher and J. Qiu, "Ultralytics YOLO11," 2024. [Online]. Available: <https://github.com/ultralytics/ultralytics>
- [29] T.-Y. Lin, M. Maire, S. Belongie, J. Hays, P. Perona, D. Ramanan, P. Dollár, and C. L. Zitnick, "Microsoft COCO: Common objects in context," in *Proc. European Conf. Computer Vision*, 2014, pp. 740–755.
- [30] P. J. Goulart and Y. Chen, "Clarabel: An interior-point solver for conic programs with quadratic objectives," 2024.
- [31] S. Diamond and S. Boyd, "CVXPY: A Python-embedded modeling language for convex optimization," *J. Machine Learning Research*, vol. 17, no. 83, pp. 1–5, 2016.
- [32] K. J. Åström and K. Furuta, "Swinging up a pendulum by energy control," *Automatica*, vol. 36, no. 2, pp. 287–295, 2000.